Nanowire surface fastener fabrication on flexible substrate

Yuhki TOKU[1], Keita UCHIDA[1], Yasuyuki MORITA[1], and Yang JU[1,*]

[1]Department of Micro-Nano Mechanical Science and Engineering, Nagoya University, Furo-cho, Chikusa-ku, Nagoya 464-8603, Japan

***Corresponding Author**

Tel: +81-52-789-4672

Fax: +81-52-789-3109

E-mail: ju@mech.nagoya-u.ac.jp

ABSTRACT. The market for wearable devices has increased considerably in recent years. According to this demand, flexible electronic circuit technology has become more important. The conventional bonding technology in electronic assembly depends on high-temperature processes such as reflow soldering, which result in undesired thermal damages and residual stress at a bonding interface. In addition, it exhibits poor compatibility with bendable or stretchable device applications. Therefore, there is an urgent requirement to attach electronic parts on printed circuit boards with good mechanical and electrical properties at room temperature. Nanowire surface

fasteners (NSFs) are candidates for resolving these problems. This paper describes the fabrication of an NSF on a flexible substrate, which can be used for room temperature conductive bonding. The template method is used for preparing high-density nanowire arrays. A Cu thin film is layered on the template as the flexible substrate. After etching the template, a Cu NSF is obtained on the Cu film substrate. In addition, the electrical and mechanical properties of the Cu NSF are studied under various fabrication conditions. The Cu NSF exhibits high shear adhesion strength (~234 N/cm^2) and low contact resistivity (2.2×10^{-4} $\Omega \cdot cm^2$).

Keywords: Nanowire, Nanowire surface fastener, Surface mount technique, Porous material, Flexible substrate

Introduction

The importance of flexible electrodes for future electronic devices has increased with the demand for wearable devices. Until now, surface mount techniques have strongly depended on soldering. However, soldering completely locks electronic components and exhibits poor compatibility with bendable or stretchable device applications. Additionally, the Pb-free solder, which was developed to prevent Pb pollution and toxicity [1-6], has been extensively researched since the Waste Electrical and Electronic Equipment and Restriction of Hazardous Substances directives. The melting point of the Pb-free solder is 20–30 °C higher than that of a conventional solder. Thus, temperature of reflow process is at least 240–250 °C, and it results in undesired thermal excursions and residual stress at a bonding interface [1, 2, 6]. The reflow process is undesirable as electric components have low thermal strength. Furthermore, once soldering is completed, it is difficult to remove the solder and components. Thus, the recycle cost tends to

become high. Therefore, there is an urgent requirement of a new bonding technique that uses a nontoxic and flexible conductive material to attach electronic parts on printed circuit boards without heating.

Biomimetic dry adhesives with conductive materials are candidates for resolving the abovementioned problems. These adhesives have attracted the attention of numerous researchers since it was reported that gecko feet consist of micro- and nanofibrillar structures [7]. Adhesive strength primarily results from the van der Waals interaction force of the large surface area of nanostructures. Thus, the gecko feet can act on an arbitrary surface, such as irregular surfaces, at room temperature. Nanostructures have adaptability on flexible surfaces; they are expected to be applied to wearable devices. Several researchers have developed biomimetic dry adhesives by fabricating nanostructures [8-14]. Qu et al. fabricated a dry adhesive that reached an adhesion force of ~100 N/cm^2 on a glass substrate using carbon nanotube arrays [8]. Kim et al. created a conductive dry adhesive using a micropillar composite of carbon nanotubes and graphene to monitor human vital signs [13]. Ko et al. presented flexible carbon nanofiber connectors, which were fabricated on a polycarbonate film. They can be used for the applications of lightweight, robust, and bendable components [11]. Even though several kinds of conductive dry adhesives have been developed, high conductivity and high adhesion strength have not yet been achieved simultaneously.

Previously, we applied the biomimetic dry adhesive technique to a surface mount technique using highly-conductive metallic nanowire (NW) arrays as an electric connector [15-19]. A pair of NW arrays attached to each other with preload works as an NW surface fastener (NSF). This technique can be applied for room temperature bonding; it can prevent undesired thermal damages at bonding interfaces and electronic components. It is easy to release NSF connection; thus,

recycling electronic components is easy. Additionally, there is no reflow process, which reduces energy consumption.

In this study, high-density Cu NW arrays are fabricated on a flexible substrate using the template method. The electrical and mechanical properties of the arrays are evaluated. The flexible substrate, which is extremely thin and easy to bend, is useful because it can be applied in a wide variety of electronic devices. Moreover, the flexible substrate is significantly lighter than Si substrates, because of which it has become essential for the downsizing of multifunction electric devices.

Method

2.1 Fabrication of Cu NSF on flexible substrate

Figure 1 shows the procedure of the template method. The advantage of this method is that NWs with homogenous length and high density can be fabricated. An anodic aluminum oxide (AAO) template was used in this study (Synkera UniKera; diameter: 13 mm; thickness: 50 μm; pore diameter: 80 nm; distance between each pore: 240 nm; pore density: 2×10^9 cm^{-2}). First, a Au thin film electrode was sputtered with thickness of approximately 100 nm on one side of the template (Fig. 1 (a)). Sputtered atoms cannot pass through the pores of the template. Thus, the Au film was fabricated as shown in Fig. 1(a). The Cu NSF was fabricated by electrodepositing Cu ions in the pores of the template (Fig. 1(b)). The electrodeposition conditions were as follows: 0.4 M $CuSO_4 \cdot 5H_2O$ aq. under a constant current of 1 mA. Additionally, we adjusted the pH of electrolyte to 2.5 using H_2SO_4. The diameter of the electrodeposition area was 9 mm. NW length was controlled by changing the electrodeposition duration. In this study, we prepared NWs with three lengths, i.e., 7.5 μm, 10 μm, and 12.5 μm. Next, a Cu thin film was electrodeposited with thickness of approximately 30 μm on the Au thin film of the AAO template as the flexible substrate

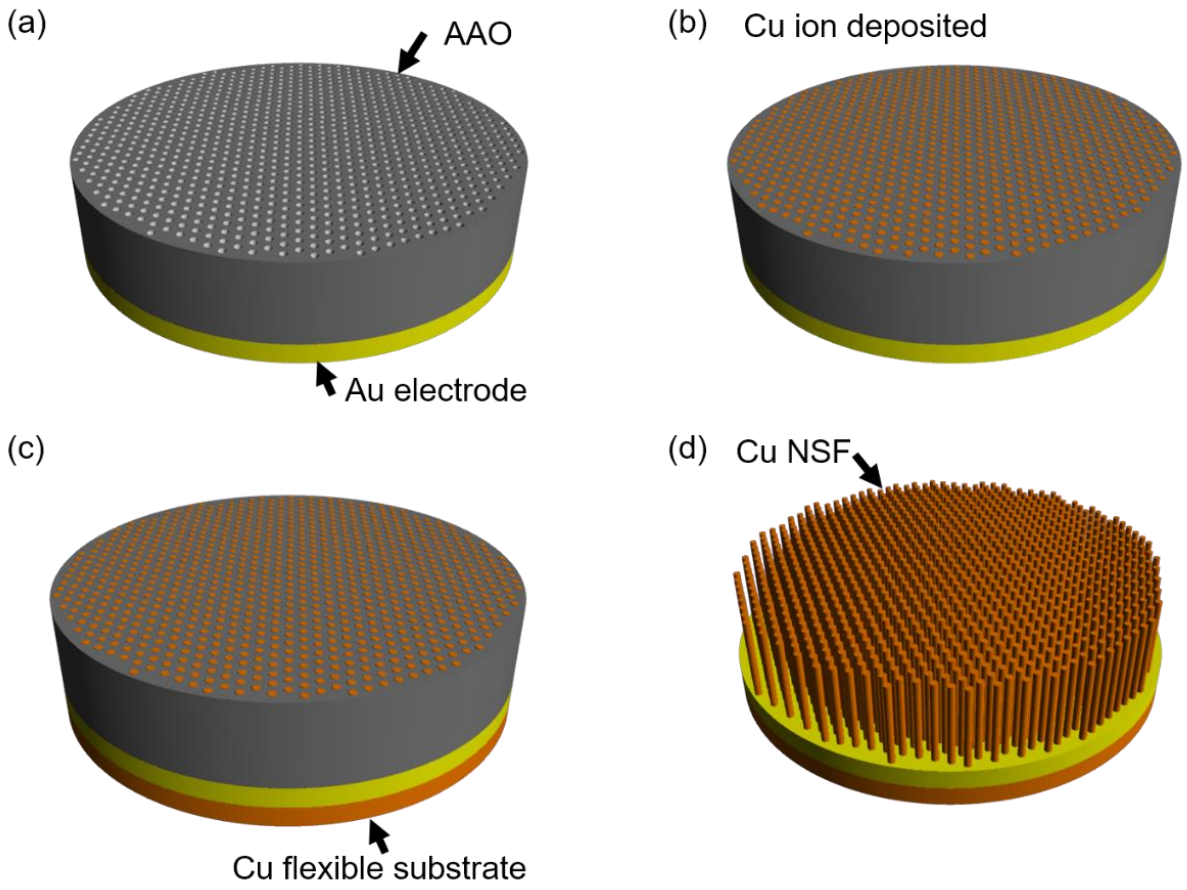

Figure 1. Procedure of template method. (a) Sputtered Au film on AAO template. (b) Electrodeposited Cu in the pores of template. (c) Electrodeposited Cu film on the Au film as a flexible substrate. (d) Etching of the AAO template.

(Fig. 1 (c)). The electrodeposition conditions were the same as those mentioned above. Here, the Au layer was used as an electrodeposition electrode to prevent surface oxidation, and the Cu layer was used to imitate the circuit on wearable materials. Then, the AAO template was etched using 3 M NaOH aq. for 1 h (Fig. 1(d)). Finally, the oxidized surface of the Cu NW was removed by employing 10 % HCl aq.

2.2 Drying method

NWs are aggregated during the natural drying process owing to the surface tension of the liquid remaining among the NWs. Thus, the influence of the aggregation on NSF properties was investigated under different drying conditions, which are shown in Table 1 [20]. In addition, we used a supercritical drying device to prevent surface tension. Supercritical drying was carried out as follows. First, the etched sample was immersed in ethanol to replace the etching solution. The sample was placed in the chamber of the supercritical drying device to replace ethanol with liquid phase CO_2. The chamber pressure and temperature were elevated to 8 MPa and 40 °C to change the CO_2 phase to a supercritical condition. Finally, the pressure was decreased to change CO_2 to a gas phase. In this study, the vapor–liquid interface was eliminated during the drying process and the nanowire array was obtained without aggregation. The NSFs fabricated under these conditions were observed through scanning electron microscopy (SEM) to confirm the difference in the extent of aggregation behaviors. Additionally, the interconnected part of the NSF was confirmed.

2.3 Evaluation of mechanical properties

First, the Cu NSF was cut into two parts with a size of approximately 1.5 mm × 5.0 mm, as shown in Fig. 2. Then, the two Cu NSFs were connected with preload, as shown in Fig. 2(a). The preload conditions were 5 N, 10 N, and 20 N. The connecting area of the Cu NSFs was approximately 1

Table 1. Drying conditions

Condition	Drying method	Temperature (℃)	Surface tension (mN/m)
1	Water	Room	78
2	Ethanol	Room	22
3	Supercritical drying	40	0

mm^2. The optical image of the adhesion strength test is shown in Fig. 2(b). One Cu NSF was fixed on a Si wafer with a weight after it was connected to another Cu NSF. The weight was placed on an electronic balance, and another Cu NSF was pulled in the upward direction. The detail of fixed Cu NSF on the Si wafer is shown in Fig. 2(c). Cu NSF adhesion strength was evaluated based on the weight measured from the difference in the values displayed on the electronic balance and the connected area of the NSFs measured by observing the nanowire array surface after the strength test with SEM. First, we investigated the influence of drying conditions on adhesion strength to determine the best condition. Then, the influence of NW length and preload was investigated using the determined drying condition.

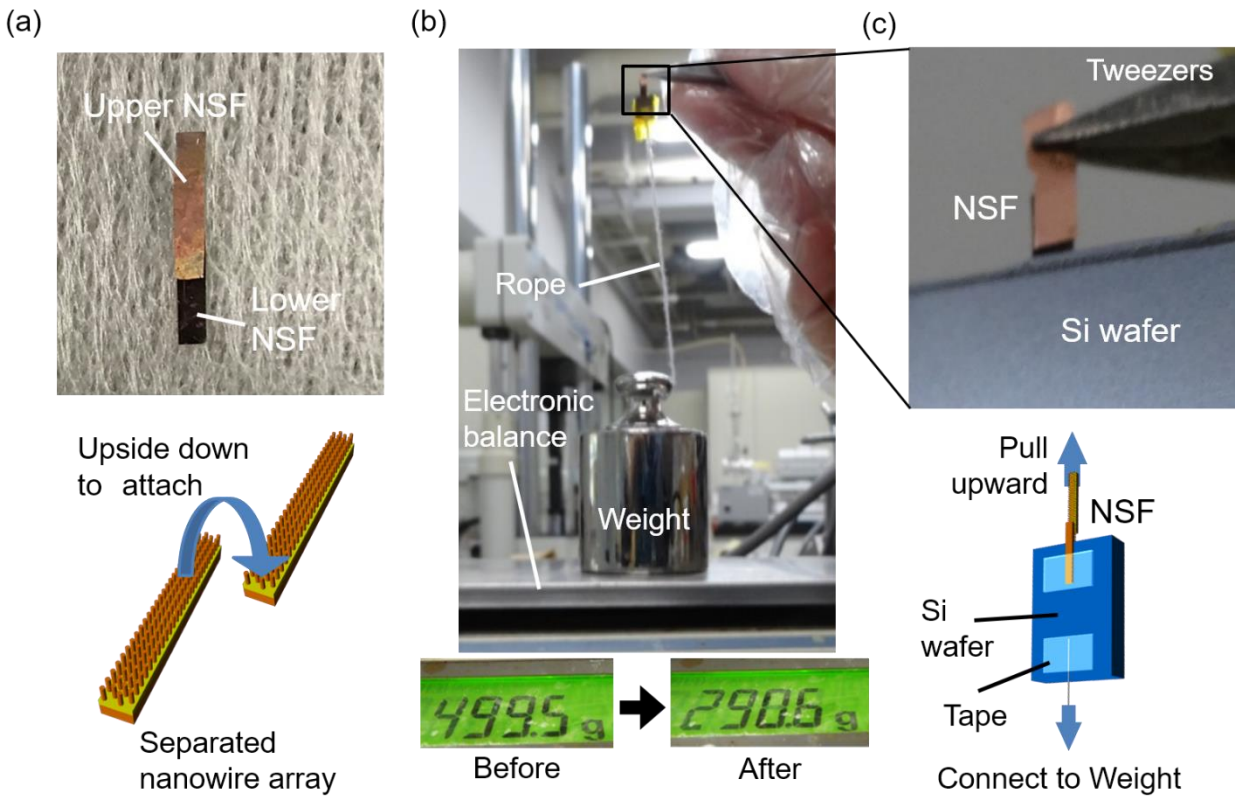

Figure 2. Images of mechanical test. (a) Connected Cu NW arrays. (b) NSF with weight pulled upward using tweezers. (c) Detail of fixed Cu NSF on Si wafer.

2.4 Evaluation of electrical properties

The schematic of electrical measurement is shown in Fig. 3. A current source (263 Calibrator/source, KEITHLEY) and a nanovoltmeter (2182A Nanovoltmeter, KEITHLEY) were used in the experiments. The electrical resistance of the Cu NSF was measured based on the V–I slope. Applied current ranged from 0 to 2.0 mA, and voltage was measured every other 0.1 mA. The measured electrical resistance, R_1, included the resistances of the Cu NSF (R_{NSF}), Cu substrate with the Au thin film ($2R_S$), and lead wires ($2R_L$) and the contact resistance ($2R_C$) between the film and lead wires, as follows:

$$R_1 = R_{NSF} + 2R_S + 2R_L + 2R_C. \quad (1)$$

$2R_c$ should be removed from R_1 to obtain the actual R_{NSF}. Thus, we measured an additional sample as shown in Fig. 3(b). This electrical resistance, R_2, includes R_S, $2R_L$, and $2R_C$, as follows:

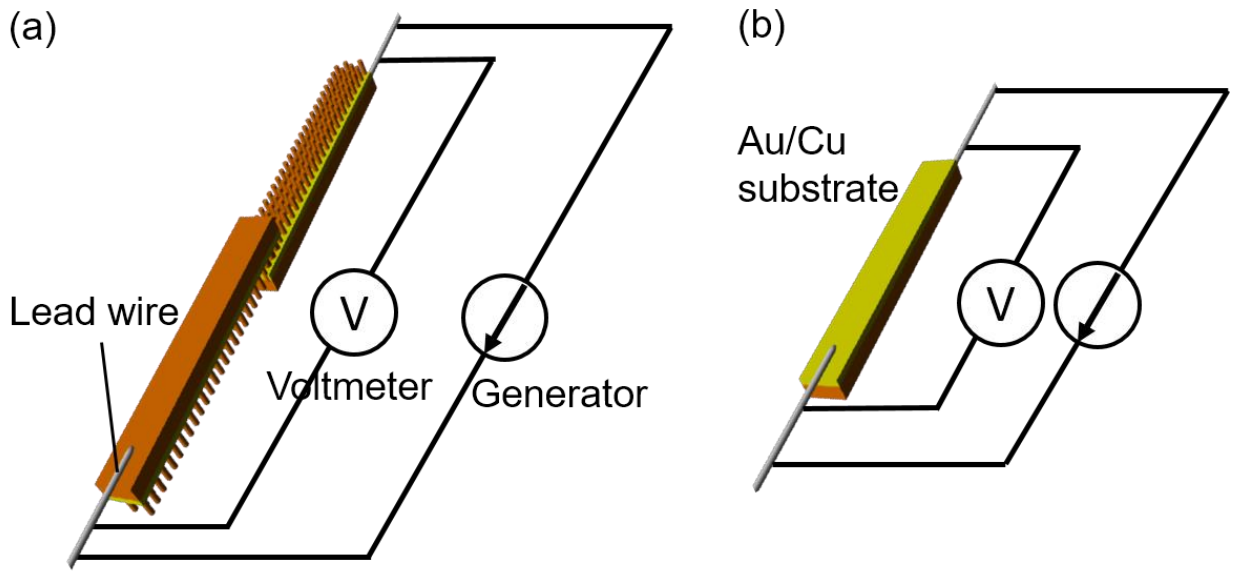

Figure 3. Schematic of electrical measurement. (a) Connected NSF. (b) Au/Cu substrate.

$$R_2 = R_S + 2R_L + 2R_C. \quad (2)$$

R_S and R_L can be neglected because they are sufficiently smaller than R_{NSF}. The electrical resistance of the Cu NSF was measured by subtracting the value in Fig. 3(b) (i.e., R_2) from that in Fig. 3(a) (i.e., R_1), as follows:

$$R_1 - R_2 = R_{NSF} + R_S \quad \text{(Note: } R_{NSF} >> R_S\text{)}. \quad (3)$$

Additionally, we introduced contact resistivity, which was expressed as the product of the measured R_{NSF} and the connecting area of the NSF (unit: $\Omega \cdot cm^2$) [21-23]. The electrical properties of the NSF were investigated by changing the preload. The drying condition and NW length were determined according to the results of mechanical properties.

Results

3.1 Cu NSF on flexible substrate

The Cu NSF was observed to be uniformly fabricated on the flexible substrate, as shown in Fig. 4. Additionally, it did not peel off from the flexible substrate even when the substrate was bent (Fig. 4). The Cu NSFs under various drying conditions were observed through SEM, as shown in Fig. 5. Under drying condition 1, NWs were aggregated and formed several NW bundles. A few NWs were tilted by more than 45°; this was caused by the surface tension among the NWs. The NWs were aggregated under drying condition 2 as well; however, the extent of aggregation was reduced. This is because the surface tension of ethanol is approximately one third of that of pure

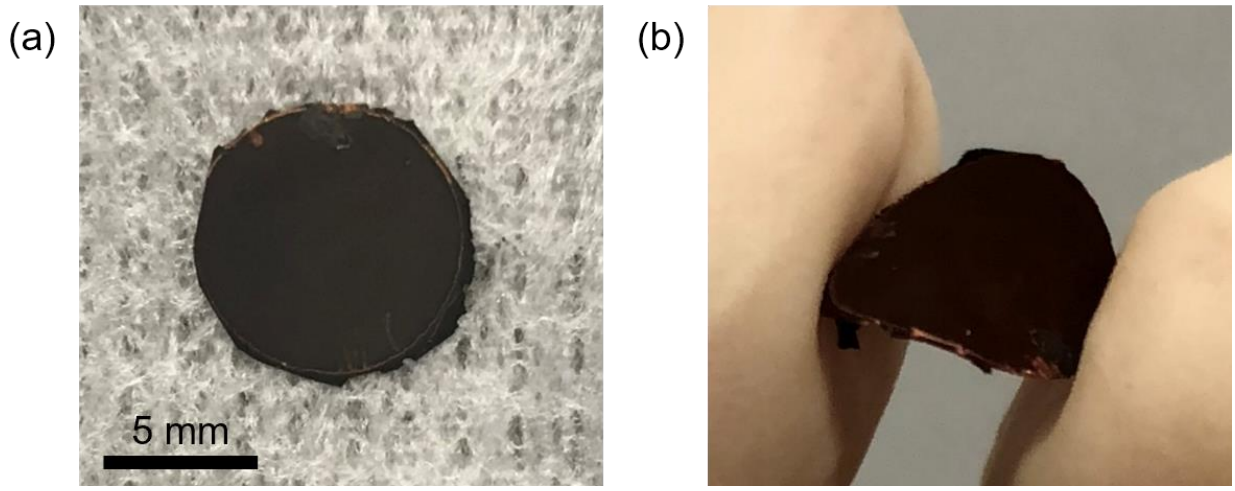

Figure 4. Cu NSF on a flexible substrate. (a) Top view of the NSF. (b) Bent NSF.

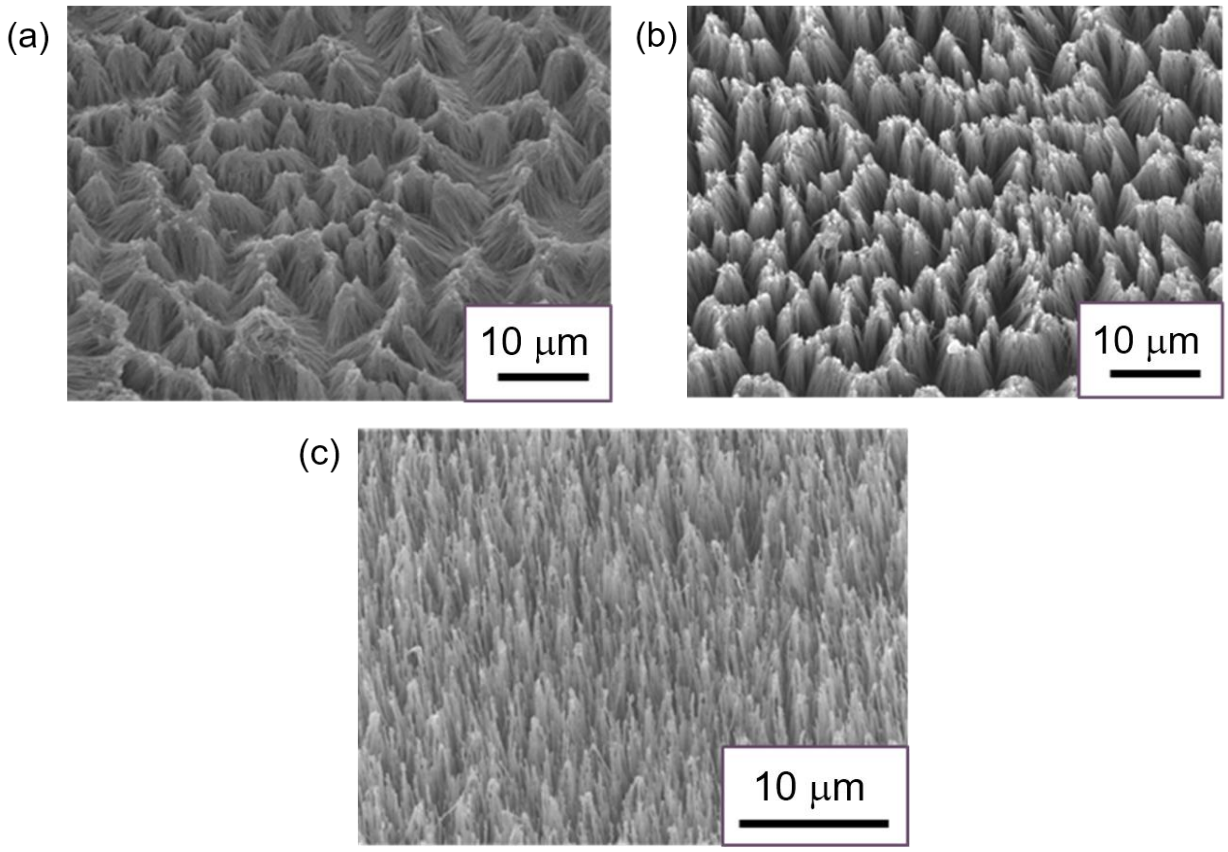

Figure 5. SEM images of NW arrays under different drying conditions. (a) Condition 1. (b) Condition 2. (c) Condition 3.

water [20]. Under drying condition 3, no bundle was observed and all NWs stood upright. According to these results, the surface tension in the drying environment strongly influences the aggregation of NW arrays during the drying process.

3.2 Evaluation of properties

The tensile test results of the NSF are shown in Fig. 6. Figure 6(a) shows the comparison of adhesion strength for different drying conditions. For each condition, Cu NSFs were connected with a NW length of 12.5 μm and a preload of 10 N. Drying condition 2 exhibited the highest adhesion strength. Thus, we used this condition for the following experiments. The adhesion strengths for NW lengths ranging from 7.5 to 12.5 μm and preloads ranging from 5 to 20 N are shown in Fig. 6(b). The maximum adhesion strengths were obtained with a preload of 10 N under all NW lengths. Figure 6(c) shows the adhesion strength for a preload of 10 N and NW lengths ranging from 7.5 to 12.5 μm. Each test was performed thrice. The average value of adhesion strength was 165 N/cm^2 and its maximum value was up to 234 N/cm^2 under the best conditions, which were a NW length of 10 μm and a preload of 10 N. It should be noted that normally the aspect ratio of the length to diameter of nanowires basically controls the load transfer [24-26]; the few change of adhesion strength with the variation of nanowire length (see Fig. 6(c)) is due to the similar interconnect length of the nanowires on the two NSFs under the same nanowire density and preload. In addition, these NSF were robust enough comparing with the adhesion strength of connected NSFs. The failure modes of the NSF such as the van der Waals force between the nanowires connection and nanowires detached from the substrate have been discussed in detail in Ref. [16].

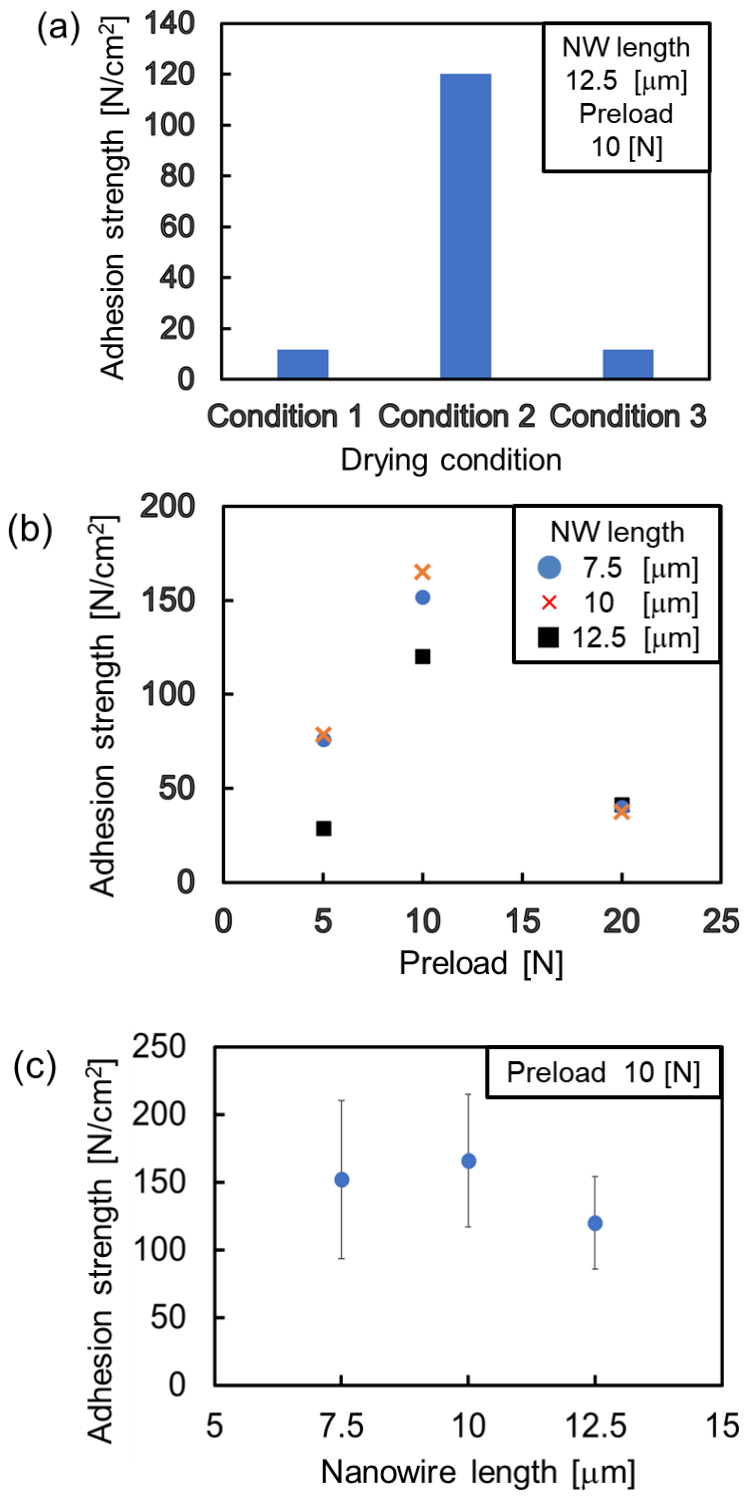

Figure 6. Adhesive strengths of NSFs for (a) different NW shapes, (b) different preloads, and (c) different NW lengths.

The results of the electrical properties tests are shown in Fig. 7. Figure 7(a) shows the relationship between the measured voltage and applied current. The samples were created under drying condition 2, and NW length was fixed as 10 μm. These conditions were determined from the results of the strength tests. Contact resistivity was calculated using the measured resistance, which was estimated from the slope of Fig. 7(a), as shown in Fig. 7(b). The best contact resistivity of the Cu NSF was 1.67×10^{-4} Ω·cm^2 under a preload of 20 N. Contact resistivity was 2.15×10^{-4} Ω·cm^2

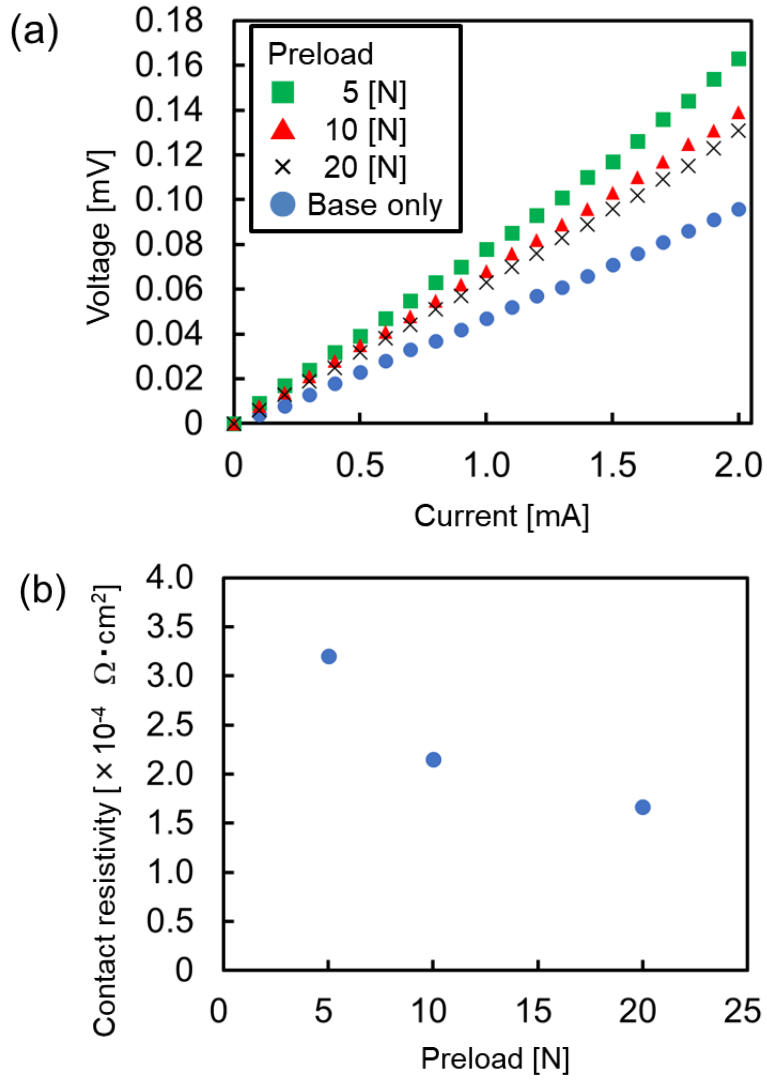

Figure 7. (a) V–I curves under different preloads. (b) Electrical resistances of Cu NSFs for different preloads.

under a preload of 10 N, which contributed to the maximum adhesion strength. Regarding to the contact resistance of nanowires it has been well described in Ref. [27-28].

Discussion

We observed the interconnection of the NSF to compare the conditions of the maximum adhesion strength (drying condition 2) and no aggregation (drying condition 3), as shown in Fig. 8. NWs penetrated each other under drying condition 2 (Fig. 8(a)) because there was sufficient space owing to aggregation. The tips of the NWs collided in each NW array under drying condition 3 (Fig. 8(b)). This is because the tips adhered owing to van der Waals force and the NWs were easily lay down

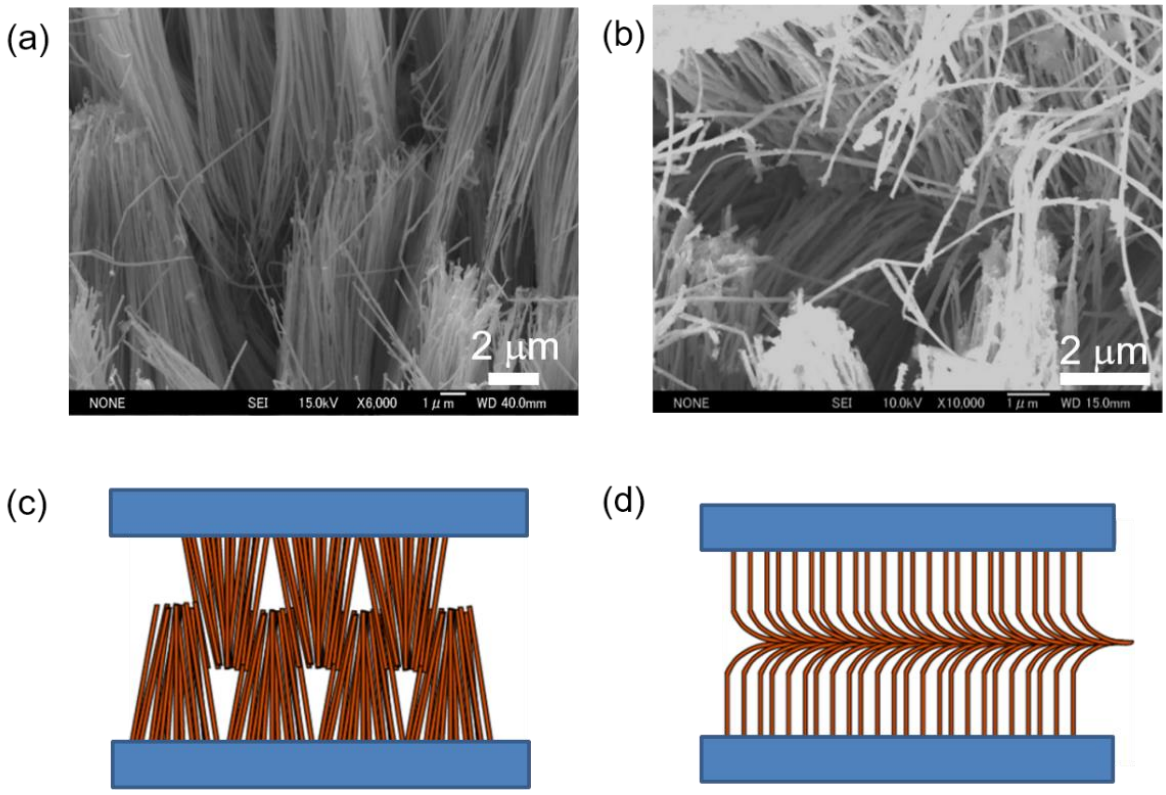

Figure 8. Cross sectional view of the NSF. (a) Interconnected NSF under drying condition 2 and (b) drying condition 3. (c) and (d) show the schematics of the cross-sectional view of (a) and (b), respectively.

on the substrate during the connection process. The surface of the NSF after the strength tests is shown in Fig. S1 in the supplementary information. The corresponding images for drying condition 2 and 3 are shown in Fig. S1 (a) and Fig. S1 (b). On comparing these two images it is observed that the bundles of NWs became loose in drying condition 2 and the NWs lay down in drying condition 3. Hence, it is possible that the NWs became mechanically entangled and adhesion strength became higher in drying condition 2 than drying condition 3 as shown in Fig. 6(a). Additionally, the NW arrays were completely compressed in the case of high preload (20 N); this increased electrical conductivity because the interspace among the NWs decreased. However, this preload is extremely high, and it possibly broke the NW structures. Thus, adhesion strength decreased in this case. For reference, the surface of the NSF after the strength tests with different preloads is also shown in Fig. S2 in the supplementary information. It should be noted that the interface of the interconnected nanowires determines the adhesion strength of the NSFs. The concept of nanowire interface has been well described in Ref. [29]; the adhesion strength affected by the connected interface which is determined by the connected angle and dimensions of the nanowires has been discussed in detail in Ref. [16]. Moreover, long-term stability of the NSF, especially oxidation, should also be considered because Cu nanowires are easily oxidized [30-32].

Table 2 shows the comparison of the NSF properties obtained in this study and in recent works. We achieved the highest adhesion strength and lowest contact resistivity by employing the flexible substrate for room temperature conductive bonding. This was possibly because the flexible substrate can help in transmitting preload compared to a rigid substrate (for example, Wang, P. et al. fabricated an NSF on a glass substrate [17]). Effective high preload contributed to high adhesion strength and electrical conductivity because the interpenetration of the NSF increased.

Table 2. Comparison of NSF properties

Ref.	Material	Adhesion shear strength (N/cm^2)	Electrical resistivity ($\Omega \cdot cm^2$)
This work	Cu NSF(on flexible substrate)	234	2.2×10^{-4}
[9]	Ge /Parylene connectors	163	None
[10]	Ge/Parylene/Ag connectors	30	1.25×10^{-1}
[16]	Cu/Parylene NSFs	25	4.22×10^{-2}
[18]	CNT array + Cu/Parylene NW array	51	1.43

In the case of an application for wearable devices, the Cu flexible substrate should be formed as a circuit on the wearable material by a photolithography technique. The NSFs should only be fabricated on electrode pads on the circuit by controlling the resist pattern. In addition, the wearable material, i.e. the supporting base of the circuit, should also be carefully selected to withstand electrodeposition process; for example, PDMS is a candidate as wearable material. Furthermore, the unique NSF structure could also be used for energy harvesting with the surface functionalization [33-36].

Conclusions

In this study, a high-density Cu NW surface fastener (NSF) was fabricated on a flexible substrate using the template method. The Cu NSF was observed through SEM, and its mechanical and electrical properties were studied under various fabrication conditions. It was observed that the adhesion strength of the Cu NSF strongly depended on the extent of aggregation of NWs. The highest adhesion strength was 234 N/cm^2 under a surface tension of 22 mN/m for drying, a NW

length of 10 μm, and a preload of 10 N. Additionally, electrical resistance was 2.2×10^{-4} Ω·cm^2 under the same condition. These results indicated that the performance of the Cu NSF is superior compared to that obtained in other studies on room temperature bonding techniques. The NSF is expected to be applied to surface mount techniques for flexible electronic devices.

Contributions

Y.T., K.U., Y.M., and Y.J. designed the research project; K.U. performed the experiments; Y.T., Y.M., and Y.J. analyzed the data; Y.T. and K.U. prepared the figures; Y.T., K.U., Y.M., and Y.J. drafted the manuscript.

Competing financial interests

The authors declare no competing financial interests.

Acknowledgment

This work was supported by the Japan Society for the Promotion of Science under Grants-in-Aid for Scientific Research (S) 17H06146.

References

1. Abtew, M. & Selvaduray, G. Lead-free solders in microelectronics. *Mater. Sci. Eng. R Rep.* **27**, 95–141 (2000).
2. Harrison, M.R., Vincent, J.H. & Steen, H.A.H. Lead-free reflow soldering for electronics assembly. *Solder. Surf. Mount Technol.* **13**, 21–38 (2001).

3. Su, Y.A., Tan, L.B., Tee, T.Y. & Tan, V.B.C. Rate-dependent properties of Sn-Ag-Cu based lead-free solder joints for WLCSP. *Microelectron. Reliab.* **50**, 564–576 (2010).
4. Keller, J., Baither, D., Wilke, U. & Schmitz, G. Mechanical properties of Pb-free SnAg solder joints. *Acta. Mater.* **59**, 2731–2741 (2011).
5. Rani, S.D. & Murthy, G.S. Evaluation of bulk mechanical properties of selected lead-free solders in tension and in shear. *J. Mater. Eng. Perform.* **22**, 2359–2365 (2013).
6. Aksöz, N., Öztürk, E., Bayram, U., Aksöz, S., Kervan, S., Ülgen A. & Maraşlı, N. Thermal conductivity variation with temperature for lead-free ternary eutectic solders. *J. Electron. Mater.* **42**, 3573–3581 (2013).
7. Autumn, K., Liang, Y.A., Hsieh, S.T., Zesch, W., Chan, W.P., Kenny, T.W., Fearing, R. & Full, R.J. Adhesive force of a single gecko foot-hair. *Nature*. **405**, 681–685 (2000).
8. Qu, L. Dai, L. Stone, M. Xia, Z. & Wang, Z. L. Carbon nanotube arrays with strong shear binding-on and easy normal lifting-off. *Science*. **322**, 238–242 (2008).
9. Ko, H., Lee, J., Schubert, B.E., Chueh, Y.-L., Leu, P.W., Fearing, R.S. & Javey, A. Hybrid core-shell nanowire forests as self-selective chemical connectors. *Nano Lett*. **9**, 2054–2058 (2009).
10. Kapadia, R., Ko, H., Chueh, Y.-L., Ho, J.C., Takahashi, T., Zhang, Z. & Javey, A. Hybrid core-multishell nanowire forests for electrical connector applications. *Appl. Phys. Lett*. **94**, 263110-1–263110-3 (2009).
11. Ko, H., Zhang, Z., Ho, J.C., Takei, K., Kapadia, R., Chueh, Y.L., Cao, W., Cruden, B.A. & Javey, A. Flexible carbon-nanofiber connectors with anisotropic adhesion properties. *Small*. **6**, 22–26 (2010).
12. Wang, Y., Hu, H., Shao, J. & Ding, Y. Fabrication of well-defined mushroom-shaped

structures for biomimetic dry adhesive by conventional photolithography and molding. *ACS Appl. Mater. Inter.* **6**, 2213–2218 (2014).

13. Kim, T., Park, J., Sohn, J., Cho, D. & Jeon, S. Bioinspired, highly stretchable, and conductive dry adhesives based on 1D-2D hybrid carbon nanocomposites for all-in-one ECG electrodes. *ACS. Nano.* **10**, 4770–4778 (2016).
14. Du, T., Ma, S., Pei, X., Wang, S. & Zhou, F. Bio-inspired design and fabrication of micro/nano-brush dual structural surfaces for switchable oil adhesion and antifouling. *Small*. **13**, 1602020-1–1602020-10 (2017).
15. Ju, Y., Amano, M. & Chen, M. Mechanical and electrical cold bonding based on metallic nanowire surface fasteners. *Nanotechnol*. **23**, 365202-1–365202-6 (2012).
16. Wang, P., Ju, Y., Cui, Y. & Hosoi, A. Copper/parylene core/shell nanowire surface fastener used for room-temperature electrical bonding. *Langmuir*, **29**, 13909–13916 (2013).
17. Wang, P., Ju, Y., Chen, M., Hosoi, A., Song, Y. & Iwasaki, Y. Room-temperature bonding technique based on copper nanowire surface fastener. *Appl. Phys. Express*. **6**, 035001-1–035001-4 (2013).
18. Cui, Y., Ju, Y., Wang, P., Xu, B., Kojima, N., Ichioka K. & Hosoi, A. Carbon nanotube-Cu/parylene nanowire array electrical fasteners with high adhesion strength. *Appl. Phys. Express*. **7**, 015102-1–015102-4 (2014).
19. Wang, P., Ju, Y. & Chen, M. Room-temperature electrical bonding technique based on copper/polystyrene core/shell nanowire surface fastener. *Appl. Surf. Sci*. **349**, 774–779 (2015).
20. Vazquez, G., Alvarez, E. & Navaza, J.M. Surface tension of alcohol + water from 20 to 50 °C. *J. Chem. Eng. Data.* **40**, 611–614 (1995).

21. Berger, H.H. Contact resistance and contact resistivity. *J. Electrochem. Soc.* **119**, 507–514 (1972).

22. Tong, T., Zhao, Y., Delzeit, L., Kashani, A. & Majumdar, A. Multiwalled carbon nanotube/nanofiber arrays as conductive and dry adhesive interface materials. *Proc. NANO 2004*. 7–12 (2004).

23. Nagashio, K., Nishimura, T., Kita, K. & Toriumi, A. Contact resistivity and current flow path at metal/graphene contact. *Appl. Phys. Lett.* **97**, 143514-1–143514-3 (2010).

24. Galan, U., Lin, Y., Ehlert, G.J. & Sodano, H.A. Effect of ZnO morphology on the interfacial strength of nanowire coated carbon fibers. *Compos. Sci. Technol.* **71**, 946–954 (2011).

25. Malakooti, M.H., Hwang, H.S. & Sodano, H.A. Morphology-controlled ZnO nanowire arrays for tailored hybrid composites with high damping. *ACS Appl. Mater. Interfaces.* **7**, 332–339 (2015).

26. Hwang, H.S., Malakooti, M.H. & Sodano, H.A. Tailored interyarn friction in aramid fabrics through morphology control of surface grown ZnO nanowires. *Compos. Part A.* **76**, 326–333 (2015).

27. Lee, J., Lee, I., Kim, T.S. & Lee, J.Y. Efficient welding of silver nanowire networks without post-processing. *Small.* **9**, 2887–2894 (2013).

28. Jang, J., Hyun, B.G., Ji, S., Cho, E., An, B.W., Cheong, W.H. & Park, J.U. Rapid production of large-area, transparent and stretchable electrodes using metal nanofibers as wirelessly operated wearable heaters. *NPG Asia Mater.* **9**, e432 (2017).

29. Malakooti, M.H., Zhou, Z., Spears, J.H., Shankwitz, T.J. & Sodano, H.A. Biomimetic nanostructured interfaces for hierarchical composites. *Adv. Mater. Interfaces.* **3**, 1500404-1–1500404-9 (2016).

30. Han, S., Hong, S., Ham, J., Yeo, J., Lee, J., Kang, B., Lee, P., Kwon, J., Lee, S.S., Yang, M.Y. & Ko, S.H. Fast plasmonic laser nanowelding for a Cu-nanowire percolation network for flexible transparent conductors and stretchable electrodes. *Adv. Mater.* **26**, 5808–5814 (2014).

31. Oh, S.J., Kim, T.G., Kim, S.Y., Jo, Y., Lee, S.S., Kim, K., Ryu, B.H., Park, J.U., Choi, Y. & Jeong, S. Newly designed Cu/Cu10Sn3 core/shell nanoparticles for liquid phase-photonic sintered copper electrodes: large-area, low-cost transparent flexible electronics. *Chem. Mater.* **28**, 4714–4723 (2016).

32. Kim, H., Choi, S.H., Kim, M., Park, J.U., Bae, J. & Park, J. Seed-mediated synthesis of ultra-long copper nanowires and their application as transparent conducting electrodes. *Appl. Surf. Sci.* **422**, 731–737 (2017).

33. Qin, Y., Wang, X. & Wang, Z.L. Microfibre-nanowire hybrid structure for energy scavenging. *Nature.* 451, 809–813 (2008).

34. Malakooti, M.H., Patterson, B.A., Hwang, H.S. & Sodano, H.A. ZnO nanowire interfaces for high strength multifunctional composites with embedded energy harvesting. *Energy Environ. Sci.* **9**, 634–643 (2016).

35. Xie, Y., Ju, Y. Toku, Y. & Morita, Y. Fabrication of Fe_2O_3 nanowire arrays based on oxidation-assisted stress-induced atomic-diffusion and their photovoltaic properties for solar water splitting, *RSC Adv.* **7**, 30548–30553 (2017).

36. Xie, Y., Ju, Y. Toku, Y. & Morita, Y. Synthesis of a single-crystal Fe_2O_3 nanowire array based on stress-induced atomic diffusion used for solar water splitting. Royal Society Open Sci. **5**, 172126-1–172126-10 (2018).